

Unsplit superconducting and time reversal symmetry breaking transitions in Sr_2RuO_4 under hydrostatic pressure and disorder.

Vadim Grinenko,^{1,2,*} Debarchan Das,³ Ritu Gupta,³ Bastian Zinkl,⁴ Naoki Kikugawa,⁵ Yoshiteru Maeno,⁶ Clifford W. Hicks,^{7,8} Hans-Henning Klauss,¹ Manfred Sigrist,^{4,†} and Rustem Khasanov^{3,‡}

¹*Institute for Solid State and Materials Physics,*

Technische Universität Dresden, D-01069 Dresden, Germany

²*Leibniz-Institut für Festkörper- und Werkstoffforschung (IFW) Dresden, D-01171 Dresden, Germany*

³*Laboratory for Muon Spin Spectroscopy, Paul Scherrer Institut, CH-5232 Villigen PSI, Switzerland*

⁴*Institute for Theoretical Physics, ETH Zurich, CH-8093 Zurich, Switzerland*

⁵*National Institute for Materials Science, Tsukuba 305-0003, Japan*

⁶*Department of Physics, Kyoto University, Kyoto 606-8502, Japan*

⁷*Max Planck Institute for Chemical Physics of Solids, D-01187 Dresden, Germany*

⁸*School of Physics and Astronomy, University of Birmingham, Birmingham B15 2TT, United Kingdom*

There is considerable evidence that the superconducting state of Sr_2RuO_4 breaks time reversal symmetry. In the experiments showing time reversal symmetry breaking its onset temperature, T_{TRSB} , is generally found to match the critical temperature, T_c , within resolution. In combination with evidence for even parity, this result has led to consideration of a $d_{xz} \pm id_{yz}$ order parameter. The degeneracy of the two components of this order parameter is protected by symmetry, yielding $T_{\text{TRSB}} = T_c$, but it has a hard-to-explain horizontal line node at $k_z = 0$. Therefore, $s \pm id$ and $d \pm ig$ order parameters are also under consideration. These avoid the horizontal line node, but require tuning to obtain $T_{\text{TRSB}} \approx T_c$. To obtain evidence distinguishing these two possible scenarios (of symmetry-protected versus accidental degeneracy), we employ zero-field muon spin rotation/relaxation to study pure Sr_2RuO_4 under hydrostatic pressure, and $\text{Sr}_{1.98}\text{La}_{0.02}\text{RuO}_4$ at zero pressure. Both hydrostatic pressure and La substitution alter T_c without lifting the tetragonal lattice symmetry, so if the degeneracy is symmetry-protected T_{TRSB} should track changes in T_c , while if it is accidental, these transition temperatures should generally separate. We observe T_{TRSB} to track T_c , supporting the hypothesis of $d_{xz} \pm id_{yz}$ order.

INTRODUCTION

For unconventional superconductors identifying the symmetry of the order parameter is crucial to pinpoint the origin of the superconductivity. Unconventional pairing states are distinguished from conventional ones by a non-trivial intrinsic phase structure which causes additional spontaneous symmetry breaking at the superconducting phase transition. This can lead, for instance, to a reduction of the crystal symmetry or the loss of time reversal symmetry. Indeed, several superconductors are known, which show experimental responses consistent with time reversal symmetry breaking (TRSB) superconductivity [1–11].

TRSB superconducting states are formed by combining two or more order parameter components with complex coefficients. These components may be degenerate by symmetry, belonging to a single irreducible representation of the crystalline point group (as in the case of $p_x \pm ip_y$ or $d_{xz} \pm id_{yz}$ superconductivity on a tetragonal lattice), or they may come from different representations (for example, $d_{xy} \pm id_{x^2-y^2}$ superconductivity on a tetragonal lattice). In the following, we refer to the former as *single-representation* and the latter as *composite-representation* order parameters. For composite-representation order parameters, the two components will generally onset at different temperatures. The higher transition temperature becomes T_c , the superconducting critical temperature, and the lower temperature T_{TRSB} , the temperature where time re-

versal symmetry breaking onsets. The possibility of composite order parameters is usually dismissed out of hand, because it is unusual for two components that are not related by symmetry to be close enough in energy. However, there are a few known examples: s and $d_{x^2-y^2}$ are relatively close in energy in iron-based superconductors [11, 12], while both (U,Th)Be₁₃[1, 4] and UPt₃[2, 3, 8] have split T_c and T_{TRSB} .

Here, we study Sr_2RuO_4 , an unconventional superconductor [13, 14], in which the origin of the superconductivity remains a mystery. Evidence that this superconductor breaks time reversal symmetry comes from zero-field muon spin rotation/relaxation (ZF- μ SR) experiments [15] and polar Kerr effect measurements [16]. Phase-sensitive probes using a corner SQUID device give further support [17]. Moreover, the Josephson effect between a conventional superconductor and Sr_2RuO_4 reveal features compatible with the presence of superconducting domains, as expected for TRSB superconductivity [18–20]. For two decades the leading candidate state to explain these and other observations was the chiral p -wave state $p_x \pm ip_y$ (the lattice symmetry of Sr_2RuO_4 is tetragonal), which has odd parity and therefore equal spin pairing. However, there is compelling evidence against an order parameter with such spin structure. This evidence includes paramagnetic limiting for in-plane magnetic fields [21–23] and the recently discovered drop in the NMR Knight shift below T_c [24, 25]. In combination with the above experimental support for TRSB superconductivity, this evidence compels consideration of $d_{xz} \pm id_{yz}$

order.

$d_{xz} \pm id_{yz}$ order would be a surprise because it has a line node at $k_z = 0$, which under conventional understanding requires interlayer pairing, while in Sr_2RuO_4 interlayer coupling is very weak. It has been proposed that $d_{xz} \pm id_{yz}$ order might be obtained through multi-orbital degrees of freedom; in this model the order parameter symmetry is encoded in orbital degrees of freedom, so interlayer pairing is not required [26]. This form of pairing is also under consideration for URu_2Si_2 [27, 28]. However, so far it has not been unambiguously confirmed in any material. To avoid horizontal line nodes, the composite-representation order parameters $s \pm id_{x^2-y^2}$ [29], $s \pm id_{xy}$ [30] and $d_{x^2-y^2} \pm ig_{xy(x^2-y^2)}$ [31, 32] have also recently been proposed for Sr_2RuO_4 . In contrast to $d_{xz} \pm id_{yz}$, these require tuning to obtain $T_c \approx T_{\text{TRSB}}$ on a tetragonal lattice.

In this work, to test whether the order parameter of Sr_2RuO_4 is of single- or composite-representation type we perform ZF- μSR measurements on hydrostatically pressurised Sr_2RuO_4 and on La-doped $\text{Sr}_{2-y}\text{La}_y\text{RuO}_4$. Both of these perturbations maintain the tetragonal symmetry of the lattice. If the order parameter has single-representation nature, T_{TRSB} will therefore track T_c . If the order parameter is of the composite-representation kind, with T_{TRSB} matching T_c in clean, unstressed samples through an accidental fine tuning, then perturbations away from this point should in general split T_{TRSB} and T_c , whether they preserve tetragonal lattice symmetry or not [33]. Here, we have observed a clear suppression of T_{TRSB} at a rate matching the suppression of T_c . Our experimental results provide evidence in favour of single-representation nature of the order parameter in Sr_2RuO_4 .

EXPERIMENTAL DESIGN AND RESULTS

μSR on Sr_2RuO_4 under hydrostatic pressure

The hydrostatic pressure measurement setup is shown schematically in Fig. 1. Sr_2RuO_4 crystals of diameter $\varnothing \sim 3$ mm were affixed to oxygen-free copper foils, and assembled into an approximately cylindrical collection of total diameter $\varnothing \sim 7$ mm and total length $l \sim 12$ mm [see Fig. 1(a)]. The c -axes of the separate crystals were aligned to within 3° .

The pressure cell used in the present study [Refs. 34, 35 and Fig. 1(b)] is a modification of a ‘classic μSR ’ clamped pressure cell [35, 36]. It consists of a main body that encloses the sample and pressure medium, a teflon cap with a metallic support, a tungsten carbide piston, a pressing pad, and a clamping bolt (not shown) that holds the piston in place. All the metallic parts of the cell apart from the piston are made from a nonmagnetic beryllium-copper alloy, which is known to have a temperature-independent μSR response [34–36]. The main feature of this cell is that the only materials placed

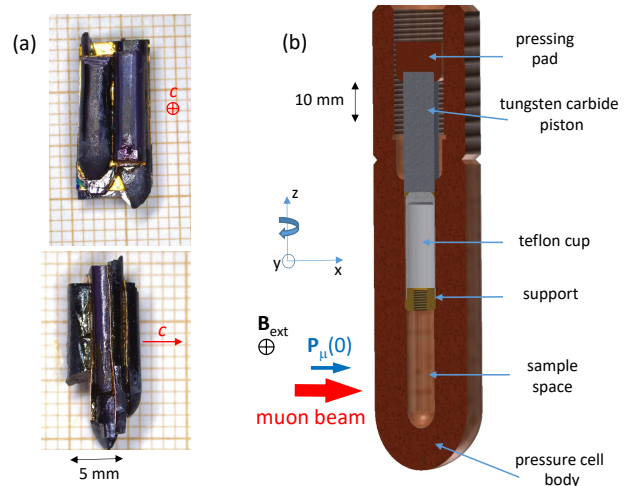


FIG. 1: Setup for hydrostatic pressure experiments. (a) Sr_2RuO_4 sample, consisting of semi-cylindrical pieces glued on oxygen-free copper foils. The top and the bottom panels are the front and the side view, respectively. The crossed circle and the arrow indicate the orientation of the c -axis. (b) Construction of the pressure cell [34]. The sample and the pressure medium are surrounded only by beryllium-copper (the pressure cell body and the teflon cap support). The parts of the cell with strong μSR response (teflon cap and tungsten carbide piston) are far from the sample and outside of the muon beam. The initial muon spin polarization $\mathbf{P}_\mu(0)$ and the external field \mathbf{B}_{ext} in TF- μSR measurements are aligned along the x - and y -axes, respectively. By rotating the cell about the z -axis, the angle between $\mathbf{P}_\mu(0)$ and the sample c -axis can be varied.

in the muon beam are the sample, the pressure medium, and this CuBe alloy. The muons had a typical momentum of 97 MeV/c, sufficient to penetrate the walls of the pressure cell. The pressure medium was 7373 Daphne oil, which at room temperature solidifies at a pressure $p \approx 2.3$ GPa [37]. The maximum pressure reached here was 0.95 GPa, and therefore hydrostatic conditions are expected. The pressure was determined by monitoring the critical temperature of a small piece of indium (the pressure indicator) placed inside the cell with the Sr_2RuO_4 sample. Confirmation that essentially hydrostatic conditions were attained is provided by the fact that T_c was observed to decrease linearly with pressure, whereas in-plane uniaxial stress on a GPa scale causes a strong non-linear increase in T_c [38].

The samples used here were grown by the standard floating-zone method [40]. Measurements of heat capacity of pieces cut from the ends of the rods used here revealed an average T_c of 1.30(6) K (see Fig. ED1 and the Methods section), slightly below the limit of T_c of 1.50 K for a pure sample.

T_c and T_{TRSB} were both obtained by means of μSR , ensuring that both quantities were measured for precisely the same sample volume. In the μSR method, spin-polarised muons are implanted, and their spins then precess in the local magnetic field. By collecting statistics

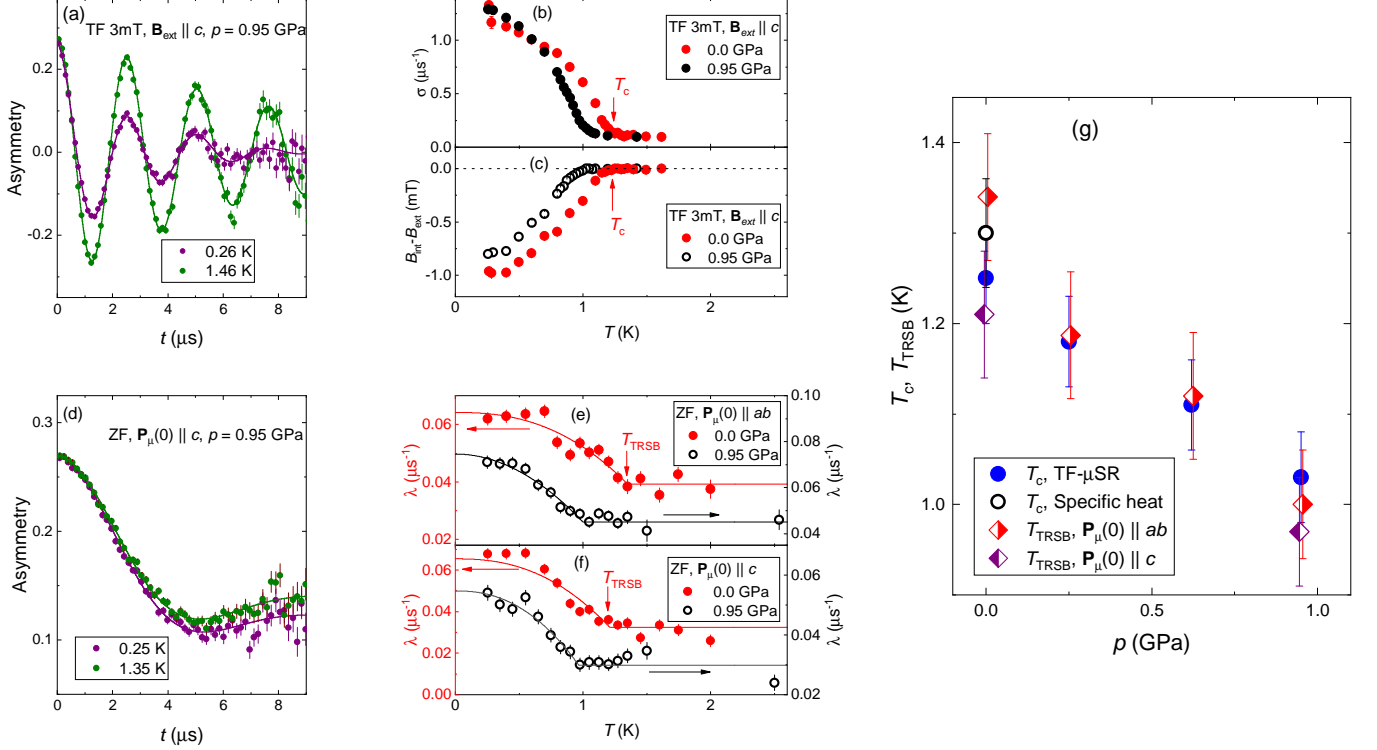


FIG. 2: Effect of pressure on T_c and T_{TRSB} in Sr_2RuO_4 . **(a)** TF- μSR time-spectra above and below T_c measured at $p = 0.95$ GPa and $B_{\text{ext}} = 3$ mT, with $\mathbf{B}_{\text{ext}} \parallel c$. The plotted quantity is the detection asymmetry between two positron detectors, which is proportional to the muon spin polarisation $P_\mu(t)$. The solid lines are fits of Eq. M1, with the sample and the pressure cell contributions described by Eqs. M2 and M3, respectively. **(b)** and **(c)** Temperature dependencies of the Gaussian relaxation rate σ and the diamagnetic shift $B_{\text{int}} - B_{\text{ext}} \propto M_{\text{FC}}$ at $p = 0.0$ and 0.95 GPa. Arrows indicate the position of the superconducting transition temperature T_c at $p = 0.0$ GPa. **(d)** ZF- μSR time-spectra above and below T_c , measured at $p = 0.95$ GPa and with initial muon spin polarisation $\mathbf{P}_\mu(0) \parallel c$. The solid lines are fits of Eq. M1, with the sample and the pressure cell parts described by Eqs. M4 and M6. **(e)** and **(f)** Temperature dependencies of the ZF exponential muon spin relaxation rate λ at $p = 0.0$ and 0.95 GPa. In panel (e), $\mathbf{P}_\mu(0) \parallel ab$, and in panel (f), $\mathbf{P}_\mu(0) \parallel c$. The solid lines are fits of Eq. 1 to the data. Arrows indicate the position of T_{TRSB} at $p = 0.0$ GPa. **(g)** Dependence of T_c and T_{TRSB} on pressure. The displayed error bars for μSR data correspond to one standard deviation from the χ^2 fit [39]. The displayed error bars for T_c indicate the rounding of the transition on a scale of approximately 0.1 K. The error bars for μSR data and T_{TRSB} correspond to one standard deviation from the χ^2 fit [39].

of decay positrons in selected direction(s), the muon polarisation as a function of time after implantation, $P_\mu(t)$, can be determined; the time-evolution of this polarisation is determined by the magnetic fields in the sample [41].

T_c is determined through transverse-field (TF) measurements. An external field B_{ext} of 3 mT was applied parallel to the crystalline c -axis and perpendicular to the initial muon spin polarization $\mathbf{P}_\mu(0)$. Measurements were performed in the field-cooled (FC) mode. Details of the method and analysis are given in the Methods section.

Example TF- μSR time spectra at pressure $p = 0.95$ GPa, and at a temperature above T_c and one below, are shown in Fig. 2(a). Above T_c , the spins of muons stopped in both the sample and the pressure cell walls precess with frequency $\omega = \gamma_\mu B_{\text{ext}}$ (where $\gamma_\mu = 2\pi \times 135.5$ MHz/T is the muon gyromagnetic ratio). The muon spin polarisation is seen to relax substantially on a 10 μs time scale. This is because approximately 50% of muons are implanted into the CuBe, where the nuclear

magnetic moments of Cu rapidly relax their polarisation. Below T_c , the internal field in the sample becomes highly inhomogeneous due to the appearance of a flux-line lattice, and so the polarisation of the muons that implanted in the sample also relaxes quickly.

TF- μSR measurements were performed at 0, 0.25, 0.62, and 0.95 GPa. Data at 0 and 0.95 GPa are shown in Fig. 2, and at the other two pressures in Figs. ED3 and ED4 in the Methods section. Data are analysed as a sum of background and sample contributions, given by Eqs. M2 and M3 (in the Methods section), respectively. From the sample contribution we extract a Gaussian relaxation rate, σ , and the diamagnetic shift of the field inside the sample, $B_{\text{int}} - B_{\text{ext}} \propto M_{\text{FC}}$ [42] (M_{FC} is the field-cooled magnetization). Figures 2 (b) and (c) respectively show the temperature dependence of σ and $B_{\text{int}} - B_{\text{ext}}$. σ is given by $\sigma^2 = \sigma_{\text{sc}}^2 + \sigma_{\text{nm}}^2$, where σ_{sc} and σ_{nm} are the flux-line lattice and nuclear moment contributions, respectively. $\sigma_{\text{sc}} \propto \lambda_{ab}^{-2}$, where λ_{ab} is the in-plane magnetic penetration depth; see Ref. 43 and the Methods

section. The onset of superconductivity can be seen in both σ and $B_{\text{int}} - B_{\text{ext}}$, as a transition rounded on a scale of approximately 0.1 K. The heat capacity measurements show a similar distribution of T_c 's; see Fig. ED1 and the Methods section.

The pressure dependence of T_c is shown in Fig. 2(g). The error bars in the figure are the rounding on the transition, and can be taken as an absolute error on T_c . When fitting $\sigma(T)$ and $B_{\text{int}}(T)$ with model functions, the statistical error on the T_c 's extracted is considerably smaller, meaning that the error on changes in T_c is low. A linear fit to $T_c(p)$ yields a slope $dT_c/dp = -0.24(2)$ K/GPa, which is in good agreement with literature data [44–46]. The unpressurised T_c is found to be 1.26(5) K, in good agreement with 1.30(6) K found in the heat capacity measurements, see the Methods section.

T_{TRSB} is determined through zero-field (ZF) measurements. The signature of time reversal symmetry breaking is an enhancement in the muon spin relaxation rate below T_{TRSB} , indicating the appearance of spontaneous magnetic fields. In these measurements, external fields were compensated to better than 2 μT , ruling out flux lines below T_c as the origin of this signal. An example of ZF- μSR time spectra above and below T_c , showing the faster relaxation below T_c , at $p = 0.95$ GPa is presented in Fig. 2(d). The pressure cell background is T -independent, so the increased signal decay comes from the sample. The sample contribution was modelled by a two-component relaxation function: $\text{GKT}(t) \cdot \exp(-\lambda t)$, in accordance with the results of Refs. 5, 6, 9, 15, 47, 48; see also the Methods section. Here, $\text{GKT}(t)$ is the Gaussian-Kubo-Toyabe function describing the relaxation of muon spin polarization in the random magnetic field distribution created by nuclear magnetic moments, and $\exp(-\lambda t)$ is a Lorentzian decay function accounting for appearance of spontaneous magnetic fields. Temperature dependencies of the exponential relaxation rate, λ , at 0 and 0.95 GPa, for independent measurements with the initial muon spin polarisation $\mathbf{P}_\mu(0) \parallel c$ and $\parallel ab$, are shown in Figs. 2(e, f); ZF data at 0.25 and 0.62 GPa are shown in Figs. ED3 and ED4 in the Methods section.

To extract T_{TRSB} , $\lambda(T)$ is fitted with the following functional form:

$$\lambda(T) = \begin{cases} \lambda_0, & T > T_{\text{TRSB}} \\ \lambda_0 + \Delta\lambda \left[1 - \left(\frac{T}{T_{\text{TRSB}}} \right)^n \right], & T < T_{\text{TRSB}} \end{cases} \quad (1)$$

λ_0 is the relaxation rate above T_{TRSB} , and $\Delta\lambda$ is the enhancement due to spontaneous magnetic fields. Where data were obtained both for $\mathbf{P}_\mu(0) \parallel c$ and $\parallel ab$, the exponent n is constrained to be the same for both polarisations. T_{TRSB} , λ_0 , and $\Delta\lambda$ were obtained independently for each pressure and muon spin polarisation. The resulting values of T_{TRSB} are plotted in Fig. 2(g).

Our ZF data yield the following three results:

(i) Where data were taken both for $\mathbf{P}_\mu(0) \parallel c$ and $\parallel ab$ (that is, at 0 and 0.95 GPa), T_{TRSB} and $\Delta\lambda$ were found

to be the same within resolution for both polarisations. [At 0 GPa, $\Delta\lambda = 0.027(4)$ and $0.033(3) \mu\text{s}^{-1}$, and at 0.95 GPa, $0.030(4)$ and $0.025(3) \mu\text{s}^{-1}$, for $\mathbf{P}_\mu(0) \parallel ab$ and $\mathbf{P}_\mu(0) \parallel c$, respectively.] This agrees with the zero-pressure results of Luke *et al.* [15]. Because $\Delta\lambda$ reflects fields perpendicular to $\mathbf{P}_\mu(0)$, this result indicates that the spontaneous fields have no preferred orientation.

(ii) $\Delta\lambda$ was found to be pressure-independent within resolution (including all pressures investigated: 0, 0.25, 0.62, and 0.95 GPa), having an average value of $\Delta\lambda = 0.026(2) \mu\text{s}^{-1}$. This value corresponds to a characteristic field strength $B_{\text{TRSB}} = \Delta\lambda/\gamma_\mu = 0.031(2)$ mT. B_{TRSB} has been found to vary from sample to sample [48], and this value is in line with previous reports [15, 47, 49, 50].

(iii) A linear fit yields $T_{\text{TRSB}}(p) = 1.27(3) \text{ K} - p \cdot 0.29(5) \text{ K/GPa}$. In other words, within resolution the rate of suppression of T_{TRSB} under hydrostatic pressure matches that of T_c .

μSR on $\text{Sr}_{1.98}\text{La}_{0.02}\text{RuO}_4$

Substitution of La for Sr adds electrons to the Fermi surfaces; in $\text{Sr}_{2-y}\text{La}_y\text{RuO}_4$ this doping drives the largest Fermi surface through a Lifshitz transition from an electron-like to a hole-like geometry, at $y \approx 0.20$ [52, 53]. At $y = 0.02$, the change in Fermi surface structure is minimal, and the main effect of the La substitution is to suppress T_c , through the added disorder. Heat capacity data, measured on a small piece cut from the μSR sample, give $T_c = 0.70(5)$ K, where the error reflects the width of the transition (see Fig. ED2).

This sample was studied at zero pressure. With no pressure cell material in the beam, the background is much smaller. The typical muon momentum was 28 MeV/c, giving of approximately 0.1 mm implantation depth [41]. Representative TF- μSR time spectra above and below T_c , where the applied field is $B_{\text{ext}} = 2$ mT parallel to the crystalline c -axis, are shown in Fig. 3(a). Below T_c , the muon spin polarisation relaxes almost completely on a 10 μs timescale, showing that essentially the entire sample volume is superconducting. The TF Gaussian relaxation rate σ is shown in panel (b), and $B_{\text{int}} - B_{\text{ext}}$ in panel (c). These measurements yield $T_c = 0.75(5)$ K. The heat capacity data are also shown in panel (b).

ZF- μSR data are presented in Figs. 3(d) and (e). Fitting with Eq. 1 returns $\Delta\lambda = 0.007(1) \mu\text{s}^{-1}$ and $T_{\text{TRSB}} = 0.8(1)$ K. This $\Delta\lambda$ is noticeably smaller than that obtained from the undoped Sr_2RuO_4 sample, corresponding to an internal field $B_{\text{TRSB}} \approx 0.01$ mT. It is, however, within the range of previous results [48]. In qualitative agreement with data on a lower- T_c Sr_2RuO_4 , reported in Ref. 47, though here with more data at $T > T_c$ to be certain of the base relaxation rate, this low value of $\Delta\lambda$ shows that B_{TRSB} is not straightforwardly related to

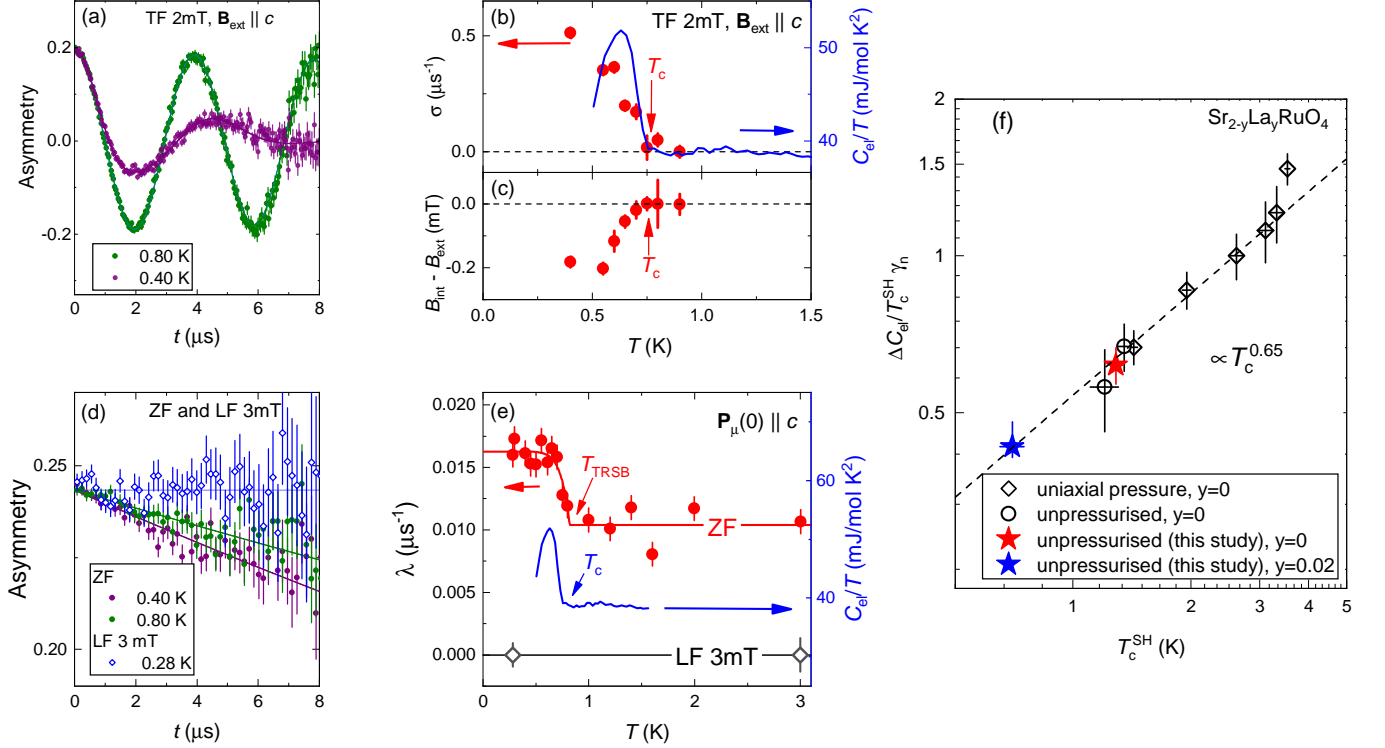


FIG. 3: TRSB in $\text{Sr}_{1.98}\text{La}_{0.02}\text{RuO}_4$. (a) TF- μSR time-spectra above and below T_c measured at $B_{\text{ext}} = 2$ mT with $\mathbf{B}_{\text{ext}} \parallel c$. The solid lines are fits of Eq. M2 to the data. (b) and (c) Temperature dependencies of the Gaussian relaxation rate σ and the diamagnetic shift $B_{\text{int}} - B_{\text{ext}}$, respectively. Arrows indicate the superconducting transition temperature T_c , determined from the TF- μSR data. The blue curve in panel (b) is the electronic specific heat C_{el}/T , measured on a small piece cut from the μSR sample. (d) ZF- and LF- μSR time-spectra. ZF data from above and below T_c , measured with $\mathbf{P}_\mu(0) \parallel c$, are shown. The LF data are from T well below T_c , and with $\mathbf{B}_{\text{ext}} = 3$ mT $\parallel \mathbf{P}_\mu(0)$. The solid lines are fits of Eq. M7. (e) Temperature dependence of the ZF and LF exponential relaxation rate λ . The solid red line is the fit of Eq. 1 to ZF $\lambda(T)$ data. The blue curve is, again, C_{el}/T . Arrows indicate positions of T_c and T_{TRSB} . (f) Double logarithmic plot of the normalized specific heat jump $\Delta C_{\text{el}}/\gamma_n T_c^{\text{SH}}$ versus T_c^{SH} [γ_n is the Sommerfeld coefficient and T_c^{SH} is the transition temperature determined from $C_{\text{el}}/T(T)$ by means of equal-entropy construction, see Fig. ED1(a)]. Filled symbols: data from this work; open symbols: data taken from Refs. 48, 51. The displayed error bars for μSR data correspond to one standard deviation from the χ^2 fit [39]. The error bars for $\Delta C_{\text{el}}/\gamma_n T_c^{\text{SH}}$ and T_c^{SH} indicate uncertainty in selecting the temperature range for linear fit below T_c .

defect density. At present, the origin of the sample-to-sample variation in B_{TRSB} is unknown.

Longitudinal-field (LF) measurements can be employed to determine whether internal fields are static or fluctuating. If B_{TRSB} is static, under an applied field parallel to $\mathbf{P}_\mu(0)$ that is considerably larger than B_{TRSB} , muon spin precession is greatly restricted and the spin polarisation does not relax (*i.e.* the muon spins decouple from B_{TRSB}). In contrast, fluctuating B_{TRSB} can still relax the muon spin polarisation [41]. Data shown in panels (d) and (e) indicate that $\mathbf{B}_{\text{ext}} \parallel \mathbf{P}_\mu(0) = 3$ mT fully suppresses the muon spin relaxation, and therefore that B_{TRSB} is static on a microsecond time scale, in agreement with data on clean Sr_2RuO_4 reported in Ref. 15. We note that LF measurements were not performed on the hydrostatically pressurised sample because the decoupling field for the Cu background is of the order of 10 mT, considerably stronger than that for Sr_2RuO_4 .

Heat capacity measurements

The specific heat measurements were performed at ambient pressure for several pieces of $\text{Sr}_{2-y}\text{La}_y\text{RuO}_4$ single crystals. The results are presented in Figs. 3 (b) and (e) for $\text{Sr}_{1.98}\text{La}_{0.02}\text{RuO}_4$ ($y = 0.02$) and in the Methods section for Sr_2RuO_4 ($y = 0$, Fig. ED1), respectively. The specific heat jumps at T_c ($\Delta C_{\text{el}}/\gamma_n T_c$, γ_n is the Sommerfeld coefficient) were further obtained in a way presented in Fig. ED2.

Figure 3 (f) summarises the $\Delta C_{\text{el}}/\gamma_n T_c^{\text{SH}}$ vs. T_c^{SH} data for our $\text{Sr}_{2-y}\text{La}_y\text{RuO}_4$ samples. Here T_c^{SH} denotes the superconducting transition temperature determined from C_{el}/T vs. T measurement curves by means of equal-entropy construction algorithm, see Fig. ED1(a) and the Methods section. In addition, we have also included some literature data for Sr_2RuO_4 with different amount of disorder [48] and for Sr_2RuO_4 under uniaxial strain [51]. In total, Fig. 3(f) compares Sr_2RuO_4 samples with a factor of five variation in T_c . Remarkably, $\Delta C_{\text{el}}/\gamma_n T_c$ vs. T_c data points scale as T_c^α with $\alpha \approx 0.65$, which is dis-

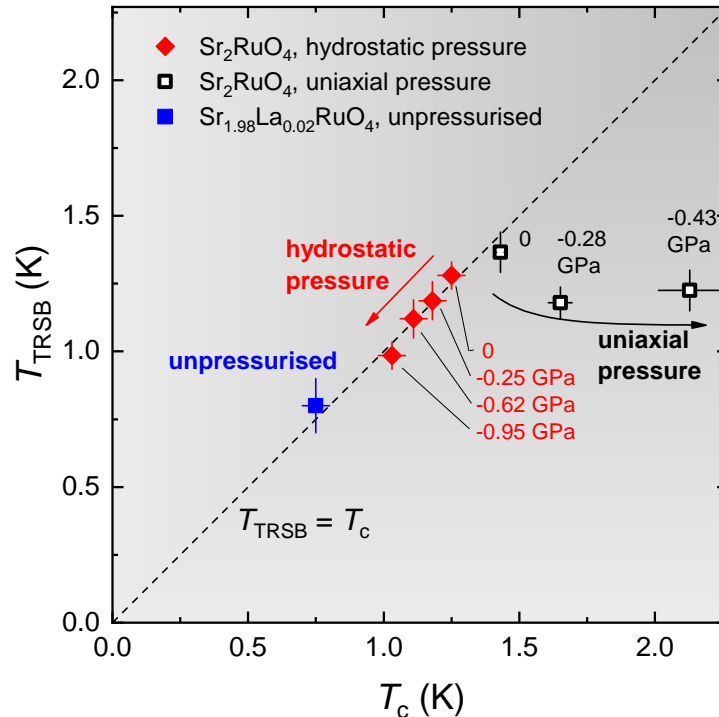


FIG. 4: Relation between T_{TRSB} and T_c . Dependence of the time reversal symmetry breaking temperature T_{TRSB} on the superconducting transition temperature T_c . The closed symbols correspond to the results obtained in present studies under hydrostatic pressure up to 0.95 GPa in pure Sr_2RuO_4 (diamonds) and in the La doped $\text{Sr}_{2-y}\text{La}_y\text{RuO}_4$ with $T_c = 0.75(5)$ K (square). The open squares are the uniaxial pressure data for undoped Sr_2RuO_4 from Ref. 48. The dashed line corresponds to $T_{\text{TRSB}} = T_c$. The minus signs at the pressure values denote the effect of ‘compression’ of the sample volume.

tinctly different from the BCS behavior, where $\alpha = 0$ ($\Delta C_{\text{el}}/\gamma_n T_c = \text{const}$). Just a single point at $T_c \simeq 3.5$ K deviates from the scaling behavior, which might be associated with tuning the electronic structure of Sr_2RuO_4 close to a van Hove singularity [51]. The results presented in Fig. 3 (f) indicate, therefore, that the perturbation changes the gap structure on the Fermi surface, i.e. its ‘anisotropy’ or the distribution among the three different bands which can lead to a renormalization of the specific heat jump being not simply proportional to normal state specific heat at T_c . Surprisingly, both hydrostatic pressure and La-doping collapse on the same curve here. The fact that this scaling is monotonic shows that both perturbations do not yield a strong qualitative change of the gap anisotropy.

It is worth noting here, that for most Fe-based superconductors, $\Delta C_{\text{el}}/\gamma_n T_c$ follows approximately the BNC (Bud’ko-Ni-Canfield) scaling behavior $\Delta C_{\text{el}}/\gamma_n T_c \propto T_c^\alpha$ with $\alpha \approx 2$ [54], which is considered to be a consequence of the unconventional multiband s_{\pm} superconductivity. The change of the superconducting pairing state in the $\text{Ba}_{1-x}\text{K}_x\text{Fe}_2\text{As}_2$ system results in abrupt change of the scaling behavior leading to an intermediate $s + is$ state [11].

DISCUSSION

In a previous ZF- μ SR experiment, in-plane uniaxial pressure, which does lift the tetragonal symmetry of the unpressurised lattice, was found to induce a strong splitting between T_c and T_{TRSB} [48]. Uniaxial pressure drives a strong increase in T_c , while T_{TRSB} varies much more weakly, probably decreasing slightly with initial application of pressure. The microscopic mechanism yielding the signal observed at T_{TRSB} , a weak enhancement in muon spin relaxation rate, remains unclear: the main proposed mechanism, magnetism induced at defects and domain walls by a TRSB superconducting order, is unproved experimentally [55, 56]. At present, the link between enhanced muon spin relaxation and TRSB superconductivity is, therefore, mainly empirical, based on: (i) the facts that it is a signal seen in only a small fraction of known superconductors, that it generally appears at T_c , and (ii) the general notion that TRSB superconductivity can in principle generate magnetic fields while muons detect magnetic fields. In Ref. 48, careful checks were performed to rule out instrumentation artefact as the origin of the signal at T_{TRSB} , and it was further argued that this signal is extremely difficult to obtain from a purely magnetic mechanism. Nevertheless, the weak observed variation of T_{TRSB} , while T_c varied strongly, raised some doubt as to whether this signal is in fact associated with

the superconductivity.

Here, we have observed a clear suppression of T_{TRSB} with hydrostatic stress, at a rate matching the suppression of T_c . This result further strengthens the evidence that enhanced muon spin relaxation is an indicator of TRSB superconductivity: T_{TRSB} tracks T_c when tetragonal lattice symmetry is preserved, while the splitting induced by uniaxial pressure shows unambiguously that it is a distinct transition, and not an artefact through some unidentified mechanism of the superconducting transition itself. Figure 4 shows T_{TRSB} versus T_c . The data reported here, on hydrostatically pressurised Sr_2RuO_4 and on unpressurised $\text{Sr}_{1.98}\text{La}_{0.02}\text{RuO}_4$, fall on the $T_{\text{TRSB}} = T_c$ line, while the uniaxial pressure data from Ref. 48 clearly deviate from this line.

Our central finding that T_{TRSB} tracks T_c provides further support for the single-representation $d_{xz} \pm id_{yz}$ order parameter. Importantly, $d_{xz} \pm id_{yz}$ is the only spin-singlet order parameter consistent with the selection rules imposed by ultrasound and Kerr effect data. The sound velocity for longitudinal ultrasound modes is renormalized at a superconducting transition, generally. A jump at T_c in ultrasound velocity for transverse modes, however, is a signature of a multi-component order parameter. Ultrasound data on Sr_2RuO_4 show precisely this type of renormalization [57, 58]. While these experimental results are not sensitive to the spin configuration, they impose other stringent conditions on the possible pairing symmetries [59, 60]. The polar Kerr effect mentioned above is a second experiment which provides symmetry-related constraints, being compatible only with chiral pairing states [16]. These two selection rules are obeyed by both the chiral p -wave and chiral d -wave state, though as noted in the Introduction, p -wave order appears to be ruled out by NMR Knight shift data [24, 25]. In contrast, the composite-representation states do not satisfy the requirements for both selection rules. The $d_{x^2-y^2} + ig_{xy(x^2-y^2)}$ and $s + id_{xy}$ states are constructed to be compatible with the ultrasound measurements, but they are not chiral [31, 61]. The $s + id_{x^2-y^2}$ state violates both selection rules [29]. It can be generally stated that any composite-representation pairing states in a tetragonal crystal, composed of components of two one-dimensional representations, would satisfy at most one of the two selection rules (see the Methods section).

Major challenges to $d_{xz} \pm id_{yz}$ order are the absence of a resolvable second heat capacity anomaly at T_{TRSB} in measurements on uniaxially pressurised Sr_2RuO_4 [51], and, as already noted, the theoretical challenges in obtaining a horizontal line node in a highly two-dimensional metal [62]. We note in addition that an analysis of low-temperature thermal conductivity data indicated vertical, rather than horizontal, line nodes in Sr_2RuO_4 [63]. The theoretical objection to horizontal line nodes may be overcome through the complex nature of the multi-orbital band structure, including sizable spin-orbit coupling [26, 64, 65].

So we may conclude that our ZF- μSR data combined

with the selection rules for ultrasound and polar Kerr effect and the NMR Knight shift behavior are consistent with the single-representation chiral $d_{xz} + id_{yz}$ -wave state, while all composite-representation states suffer from several deficiencies. We note, however, that there are also empirical challenges to a hypothesis of $d_{xz} \pm id_{yz}$, and that the difficulty in reconciling apparently contradictory experimental results in Sr_2RuO_4 may mean that one or more major, apparently solid results will in time be found to be incorrect, either for a technical reason or in interpretation. Further experiments are therefore necessary.

METHODS

Sample preparation and characterisation

$\text{Sr}_{2-y}\text{La}_y\text{RuO}_4$ single crystals

Single crystals of $\text{Sr}_{2-y}\text{La}_y\text{RuO}_4$ were grown by means of a floating zone technique [40]. Samples for measurement under hydrostatic pressure (with $y = 0$), were cut from two rods, C140 and C171, that each grew along a $\langle 100 \rangle$ crystallographic direction. The rods have diameter $\varnothing \simeq 3$ mm. Two sections of length 8–12 mm were taken from each rod. These were then cleaved, forming semi-cylindrical samples with flat surfaces perpendicular to the c -axis.

The effect of La doping on the TRSB transition was studied on a single original $\text{Sr}_{2-y}\text{La}_y\text{RuO}_4$ crystal of length 8 mm. The La concentration was analyzed by an electron-probe micro-analysis and was found to be $y \simeq 0.02$. Before the μSR measurements, this rod was then cleaved into two semi-cylindrical pieces, again with the flat faces $\perp c$.

Specific heat of $\text{Sr}_{2-y}\text{La}_y\text{RuO}_4$ at ambient pressure

Specific heat measurements were performed at zero pressure for several pieces of $\text{Sr}_{2-y}\text{La}_y\text{RuO}_4$ single crystals, cut from the rod used for μSR measurements.

For Sr_2RuO_4 used in hydrostatic pressure measurements, the electronic specific heat capacity C_{el}/T was measured for four samples: one sample cut from each end of both the C140 and C171 sections. Results are presented in Fig. ED1. The specific-heat critical temperature T_c of each sample was obtained by an equal-entropy construction, illustrated in panel (a). The spread on the critical temperature of each sample is taken as $T_{c, \text{max}} - T_{c, \text{min}}$, where $T_{c, \text{max}}$ and $T_{c, \text{min}}$ are determined for each transition as illustrated in panel (b). T_c was found to be 1.35(3) and 1.34(3) K for the two samples from rod C140, and 1.27(4) and 1.26(3) for those from C171. Because both rods were used in the hydrostatic pressure measurements, we take a combined value

$T_c^{\text{SH}} = 1.30(6)$ K for the specific-heat critical temperature of these samples together.

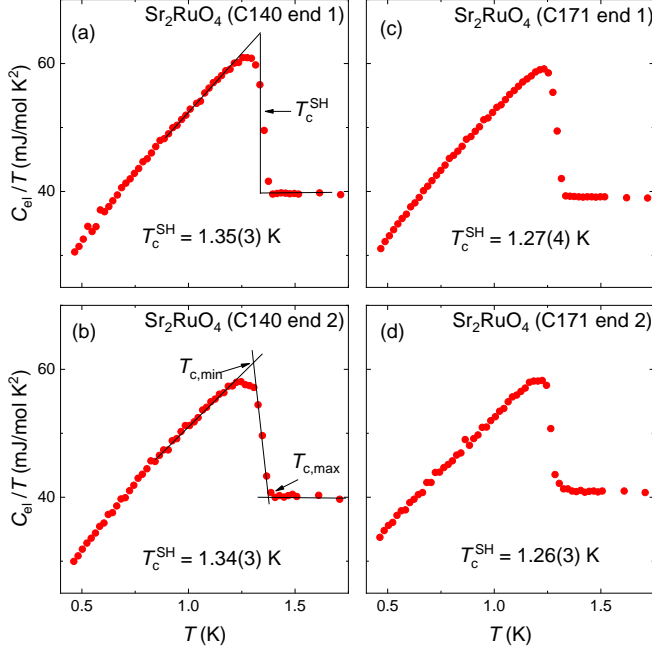


FIG. ED1: Specific heat curves taken for four ending pieces of C140 and C171 Sr_2RuO_4 rods. The mean value of the ‘specific-heat’ superconducting transition temperature T_c^{SH} is obtained by an equal-entropy construction of the idealized specific heat jump [panel (a)]. The minimum and maximum values of the transition temperature ($T_{c,\text{min}}$ and $T_{c,\text{max}}$) are determined from the crossing points of linearly extrapolated C_{el}/T vs. T curves in the vicinity of T_c [panel (b)].

The temperature dependence of C_{el}/T for a small piece cut from the $\text{Sr}_{1.98}\text{La}_{0.02}\text{RuO}_4$ μSR sample is presented in Figs. 3 (b) and (e). Figure ED2 show the same data, but with C_{el}/T normalised by the Sommerfeld coefficient γ_n . The equal-entropy construction and estimates of $T_{c,\text{min}}$ and $T_{c,\text{max}}$ result in $T_c^{\text{SH}} = 0.70(5)$ K.

μSR experiments

The muon spin rotation/relaxation (μSR) experiments were performed at the μE1 and πE1 beamlines, using the GPD [35], and Dolly spectrometers (Paul Scherrer Institute, PSI Villigen, Switzerland). At the GPD instrument, experiments under pressure up to $p \simeq 0.95$ GPa on undoped Sr_2RuO_4 were performed. At the Dolly spectrometer, measurements of $\text{Sr}_{1.98}\text{La}_{0.02}\text{RuO}_4$ at ambient pressure were conducted. At both instruments ^4He cryostats equipped with the ^3He insets (base temperature $T \simeq 0.25$ K) were used.

At the GPD instrument, measurements in zero-field (ZF- μSR) and with the field applied transverse to the initial muon spin polarization $\mathbf{P}_\mu(0)$ (TF- μSR) were performed. In two sets of ZF- μSR studies, $\mathbf{P}_\mu(0)$ was set to be parallel to the c -axis and along the ab -plane, respectively. In TF- μSR measurements the small 3 mT

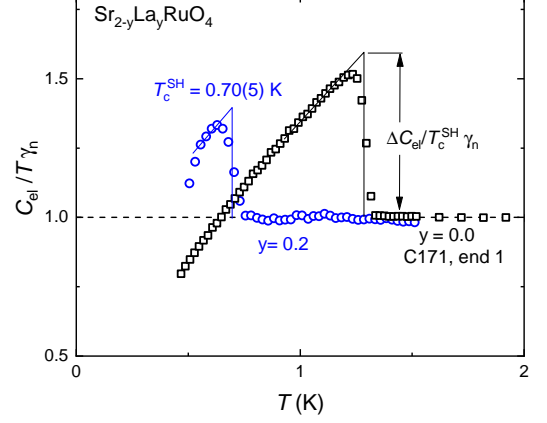


FIG. ED2: Temperature dependence of the normalized electronic specific heat $C_{\text{el}}/T\gamma_n$ measured on a small piece cut from the $\text{Sr}_{1.98}\text{La}_{0.02}\text{RuO}_4$ μSR sample (blue open circles). Open squares correspond to the $C_{\text{el}}/T\gamma_n$ vs. T data for one of Sr_2RuO_4 samples [C171, end 1; Fig. ED1(c)]. Solid lines represent an equal-entropy construction used to determine the superconducting transition temperature T_c . The double-sided arrow represent the way of determination of the specific heat jump at T_c ($\Delta C_{\text{el}}/T_c\gamma_n$).

magnetic field was applied parallel to the c -axis and perpendicular to $\mathbf{P}_\mu(0)$.

At the Dolly instrument, in addition to ZF- and TF- μSR experiments, the longitudinal-field (LF) measurements were performed. In these studies 3 mT magnetic field was applied parallel to the c -axis and to the initial muon spin polarisation $\mathbf{P}_\mu(0)$.

μSR data analysis procedure

The experimental data were analyzed by separating the μSR signal on the sample (s) and the background (bg) contributions [66]:

$$A_0 P(t) = A_s P_s(t) + A_{\text{bg}} P_{\text{bg}}(t). \quad (\text{M1})$$

Here A_0 is the initial asymmetry of the muon spin ensemble, and A_s (A_{bg}) and $P_s(t)$ ($P_{\text{bg}}(t)$) are the asymmetry and the time evolution of the muon spin polarization for muons stopped inside the sample (outside of the sample), respectively.

In a case of μSR under pressure studies, the background contribution (approximately 50% of total μSR response) is determined by the muons stopped in the pressure cell body. At ambient pressure experiment the small background contribution (of the order of 5%) is caused by muons stopped in the sample holder and the cryostat windows.

TF- μ SR

In TF- μ SR experiments, the sample contribution was analyzed by using the following functional form:

$$P_s^{\text{TF}}(t) = \exp\left[-\frac{\sigma^2 t^2}{2}\right] \cos(\gamma_\mu B_{\text{int}} t + \phi). \quad (\text{M2})$$

Here B_{int} is the internal field in the sample, ϕ is the initial phase of the muon spin ensemble, and $\gamma_\mu \simeq 2\pi \times 135.5$ MHz/T is the muon gyromagnetic ratio. The Gaussian relaxation rate σ consists of the 'superconducting', σ_{sc} , and nuclear moment, σ_{nm} , contributions and it is defined as: $\sigma^2 = \sigma_{\text{sc}}^2 + \sigma_{\text{nm}}^2$. Here, σ_{sc} and σ_{nm} characterize the damping due to the formation of the flux-line lattice in the superconducting state and of the nuclear magnetic dipolar contribution, respectively. In the analysis, σ_{nm} was assumed to be constant over the entire temperature range and was fixed to the value obtained above T_c , where only nuclear magnetic moments contribute to the muon depolarization rate [see Fig. ED3(a)].

The pressure cell contribution was described by using the following equation:

$$P_{\text{pc}}^{\text{TF}}(t) = \exp\left[-\frac{\sigma_{\text{pc}}^2 t^2}{2}\right] \cos(\gamma_\mu B_{\text{ext}} t + \phi). \quad (\text{M3})$$

Here $\sigma_{\text{pc}} \simeq 0.28 \mu\text{s}^{-1}$ is the field and the temperature independent relaxation rate of beryllium-copper [35], and B_{ext} is the externally applied field.

The solid lines in Fig. 2(a) correspond to the fit of TF- μ SR data by using Eq. M1 with the sample and the background parts described by Eqs. M2 and M3. For the data presented in Fig. 3(a) the background contribution was described by non-relaxing function $P_{\text{bg}}^{\text{TF}}(t) = \cos(\gamma_\mu B_{\text{ext}} t + \phi)$. The good agreement between the fits and the data demonstrates that the above model describes the experimental data rather well.

With the external magnetic field applied along the crystallographic c -axis ($\mathbf{B}_{\text{ext}} \parallel c$), the superconducting contribution into the Gaussian relaxation rate σ_{sc} becomes proportional to the inverse squared in-plane magnetic penetration depth λ_{ab} [43]. The proportionality coefficient between σ_{sc} and λ_{ab}^{-2} depends on the value of the applied field, the symmetry of the flux-line lattice and the angular dependence of the superconducting order parameter.

The temperature dependencies of the Gaussian relaxation rate σ and the diamagnetic shift $B_{\text{int}} - B_{\text{ext}}$ are presented in Figs. 2(b), (c) and 3(b), (c) for Sr_2RuO_4 and $\text{Sr}_{1.98}\text{La}_{0.02}\text{RuO}_4$ samples, respectively.

ZF-and LF- μ SR

The sample contribution includes both, the nuclear moment relaxation and an additional exponential relaxation λ caused by appearance of spontaneous magnetic

fields [15]:

$$P_s^{\text{ZF}}(t) = \text{GKT}_s(t) e^{-\lambda t}. \quad (\text{M4})$$

Here $\text{GKT}(t)$ is the Gaussian Kubo-Toyabe (GKT) relaxation function describing the magnetic field distribution created by the nuclear magnetic moments [41, 67]:

$$\text{GKT}(t) = \frac{1}{3} + \frac{2}{3}(1 - \sigma_{\text{GKT}}^2 t^2) e^{-\sigma_{\text{GKT}}^2 t^2/2}. \quad (\text{M5})$$

σ_{GKT} is the GKT relaxation rate.

Muons implanted in beryllium-copper pressure cell body sense solely the magnetic field distribution created by copper nuclear magnetic moments and described as:

$$P_{\text{pc}}^{\text{ZF}}(t) = \text{GKT}_{\text{pc}}(t) \quad (\text{M6})$$

with the temperature independent relaxation rate $\sigma_{\text{GKT,BeCu}} \simeq 0.35 \mu\text{s}^{-1}$ [35].

Fits of Eq. M1, with the sample and pressure cell parts described by Eqs. M4 and M6, to the ZF- μ SR data were performed globally. The ZF- μ SR time-spectra taken at each particular muon spin polarization [$\mathbf{P}_\mu(0) \parallel ab$ and $\mathbf{P}_\mu(0) \parallel c$] and pressure ($p = 0.0, 0.25, 0.62$, and 0.95 GPa) were fitted simultaneously with A_s , A_{pc} , $\sigma_{\text{GKT,Sr}_2\text{RuO}_4}$, $\sigma_{\text{GKT,BeCu}}$, and λ_0 as common parameters, and λ as individual parameter for each particular data set. The solid green and purple lines in Figs. 2 (d) correspond to the fit of ZF- μ SR data by using Eq. M1 with the sample and the background parts described by Eqs. M4 and M6.

Note that the absence of strong nuclear magnetic moments in $\text{Sr}_{2-y}\text{La}_y\text{RuO}_4$ leads to the corresponding Gaussian Kubo-Toyabe relaxation rate being nearly zero. Consequently, the analysis of ZF- and LF- μ SR data for $\text{Sr}_{1.98}\text{La}_{0.02}\text{RuO}_4$ was performed by using the simple-exponential decay function:

$$P_s^{\text{ZF,LF}}(t) = e^{-\lambda t}. \quad (\text{M7})$$

The solid lines in Figs. 3 (d) correspond to the fit of ZF- μ SR data by using Eq. M1 with the sample part described by Eqs. M7 and the non-relaxing background $P_{\text{bg}}^{\text{ZF,LF}}(t) = 1$.

The temperature dependencies of the exponential relaxation rate λ are presented in Figs. 2(e,f) and 3(e) for Sr_2RuO_4 and $\text{Sr}_{1.98}\text{La}_{0.02}\text{RuO}_4$ samples, respectively.

ZF- and TF- μ SR results at $p = 0.25$ and $p = 0.62$ GPa

Figures ED3 and ED4 show the results of TF- and ZF- μ SR measurements on Sr_2RuO_4 at $p = 0.25$ and 0.62 GPa. Arrows in panels (a) and (b) indicate the position of the superconducting transition temperature T_c . Arrow in panel (c) indicate the TRSB transition temperature T_{TRSB} .

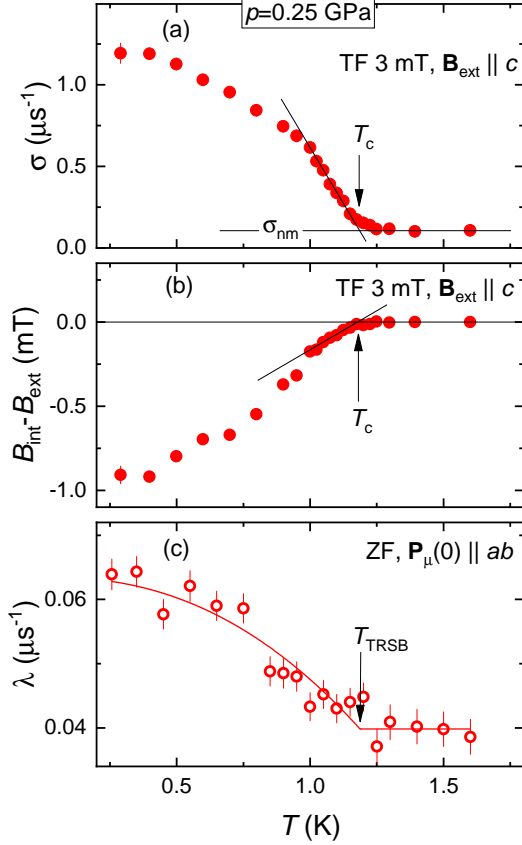


FIG. ED3: (a) Temperature dependence of the Gaussian relaxation rate σ measured at $p = 0.25$ GPa and the external field $B_{\text{ext}} = 3$ mT applied parallel to the crystallographic c -axis. (b) The diamagnetic shift of the internal field $B_{\text{int}} - B_{\text{ext}} \propto M_{\text{FC}}$ [42], M_{FC} is the field-cooled magnetization, at $p = 0.25$ GPa. Arrows in panels (a) and (b) indicate the position of the superconducting transition temperature T_c . (c) Temperature dependence of the ZF exponential relaxation rate λ induced by spontaneous magnetic fields caused by TRSB effects at $p = 0.25$ GPa. The initial muon spin polarization $\mathbf{P}_\mu(0)$ is parallel to the ab -plane. The solid line is the fit by means of Eq. 1 from the main text. Arrow indicate the position of TRSB transition temperature T_{TRSB} .

Extraction of T_c from the TF- μ SR data

The superconducting transition temperature T_c was extracted from temperature dependencies of the Gaussian relaxation rate, σ , and the diamagnetic shift of the internal field, $B_{\text{int}} - B_{\text{ext}} \propto M_{\text{FC}}$, as they obtained in TF- μ SR experiments [see Figs. 2(b,c), 3(b,c), ED3(a,b), and ED4(a,b)].

In a case of $\sigma(T)$ data, the transition temperature was defined as a crossing point of linearly extrapolated $\sigma(T)$ curve in the vicinity of T_c with $\sigma = \sigma_{\text{nm}}$ line. Note that σ_{nm} is constant over the entire temperature range and it corresponds to the value reached above T_c [see Fig. ED3(a)].

From the diamagnetic shift data, the transition temperature was defined as a crossing point of linearly extrapolated $B_{\text{int}} - B_{\text{ext}}$ vs. T curve in the vicinity of T_c

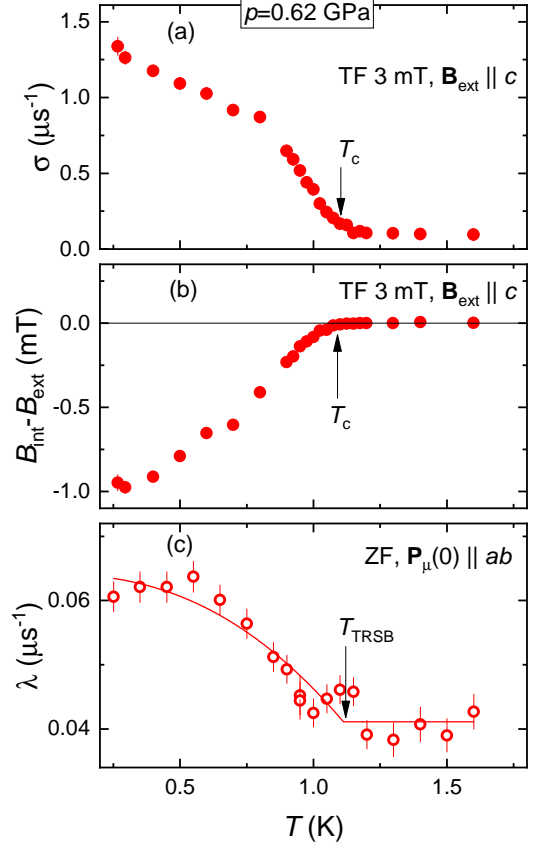


FIG. ED4: The same as in Fig. ED3 but for $p = 0.62$ GPa.

with $B_{\text{int}} - B_{\text{ext}} = 0$ line [see Fig. ED3(b)].

Symmetry properties of the order parameters

Several order parameters have been proposed for the time reversal symmetry-breaking superconducting state of Sr_2RuO_4 . We would like here to give a brief overview on the different options and the symmetry requirements to satisfy the selection rules for two experiments: ultrasound velocity renormalization for the transverse c_{66} -mode and the polar Kerr effect. For tetragonal crystal symmetry with the point group D_{4h} the even-parity spin-singlet pairing states can be listed according to the irreducible representations of D_{4h} , four one-dimensional ones $A_{1g}, A_{2g}, B_{1g}, B_{2g}$ and a two-dimensional one E_u . The pair wave function $\psi_\Gamma(\mathbf{k})$ of the corresponding states are given by

$$\begin{aligned}
 \psi_{A_{1g}}(\mathbf{k}) &= \psi_0(\mathbf{k}) & s\text{-wave} \\
 \psi_{A_{2g}}(\mathbf{k}) &= \psi_0(\mathbf{k})k_xk_y(k_x^2 - k_y^2) & g_{xy(x^2 - y^2)}\text{-wave} \\
 \psi_{B_{1g}}(\mathbf{k}) &= \psi_0(\mathbf{k})k_x^2 - k_y^2 & d_{x^2 - y^2}\text{-wave} \\
 \psi_{B_{2g}}(\mathbf{k}) &= \psi_0(\mathbf{k})k_xk_y & d_{xy}\text{-wave} \\
 \psi_{E_g}(\mathbf{k}) &= \{\psi_0(\mathbf{k})k_xk_z, \psi_0(\mathbf{k})k_yk_z\} & \{d_{xz}, d_{yz}\}\text{-wave}
 \end{aligned} \tag{M8}$$

where $\psi_0(\mathbf{k})$ is a function of \mathbf{k} invariant under all symmetry operations of the tetragonal lattice. We list here first the composite-representation TRSB states:

$$\begin{aligned}
\tilde{\Gamma}_1 &= A_{1g} \oplus A_{2g} : s + ig\text{-wave} \\
\tilde{\Gamma}_2 &= A_{1g} \oplus B_{1g} : s + id\text{-wave} \\
\tilde{\Gamma}_3 &= A_{1g} \oplus B_{2g} : s + id'\text{-wave} \\
\tilde{\Gamma}_4 &= B_{1g} \oplus A_{2g} : d + ig\text{-wave} \\
\tilde{\Gamma}_5 &= B_{2g} \oplus A_{2g} : d' + ig\text{-wave} \\
\tilde{\Gamma}_6 &= B_{1g} \oplus B_{2g} : d + id'\text{-wave}
\end{aligned} \tag{M9}$$

Note that in general different representations correspond to different critical temperature. Thus to obtain a single superconducting phase transition for the composite states an accidental degeneracy of two representations is necessary. The two states proposed so far are $\tilde{\Gamma}_2$ [29, 30] and $\tilde{\Gamma}_4$ [31, 32]. The two-dimensional representation allows for the combination

$$\tilde{\Gamma}_7 = E_g : \text{chiral } d\text{-wave} \tag{M10}$$

with a pair wave function $\psi_{E_g}(\mathbf{k}) = \psi_0(\mathbf{k})k_z(k_x \pm ik_y)$ as proposed in Refs. 26, 62. All composite states, $\tilde{\Gamma}_{1-6}$, can be constructed by electron pairing within the RuO_2 planes, while the state $\tilde{\Gamma}_7$ requires interlayer pairing. Due to the spin singlet nature all states are compatible with the new NMR Knight shift results [24, 25]. All TRSB state are expected to generate internal spontaneous currents around defects, such as surfaces and domain walls and, consequently, under present understanding are compatible with the μSR experiments [15].

Next we consider the two selection rules. For the coupling to the lattice we restrict consideration to the mode which corresponds to the elastic constant c_{66} , which is connected with the strain tensor element $\epsilon_{xy} = \epsilon_{yx}$ [59, 60]. This is active for transverse modes with a wave vector in the plane, e.g. [100] and a polarization perpendicular also within the plane. This strain tensor component belongs by symmetry to the representation B_{2g} [59, 60, 68]. For the observed renormalization of the speed of sound the superconducting order parameter has to couple linearly to ϵ_{xy} , thus, requiring that B_{2g} is contained in the decomposition of $\tilde{\Gamma}_j \otimes \tilde{\Gamma}_j$. This is only possible for $\tilde{\Gamma}_3, \tilde{\Gamma}_4$ and $\tilde{\Gamma}_7$:

$$\tilde{\Gamma}_3 \otimes \tilde{\Gamma}_3 = \tilde{\Gamma}_4 \otimes \tilde{\Gamma}_4 = 2A_{1g} \oplus 2B_{2g} \tag{M11}$$

and

$$\tilde{\Gamma}_7 \otimes \tilde{\Gamma}_7 = A_{1g} \oplus A_{2g} \oplus B_{1g} \oplus B_{2g}. \tag{M12}$$

The selection rule resulting in the polar Kerr effect requires the order parameter to couple by symmetry to the z -component of the magnetic field, B_z which belongs to the representation A_{2g} . Again we consider the decomposition of the corresponding representations of the

different pairing states. We find that only $\tilde{\Gamma}_1, \tilde{\Gamma}_6$ and $\tilde{\Gamma}_7$ satisfy the condition. The only pairing state which appears to obey both selection rules is the chiral d -wave state. None of the composite pairing states can satisfy both conditions. Among them there are the states $\tilde{\Gamma}_2$ and $\tilde{\Gamma}_5$ which are in conflict with both selection rules.

Turning to the odd-parity states the analogous picture arises with

$$\begin{aligned}
d_{A_{1u}}(\mathbf{k}) &= \psi_0(\mathbf{k})(\hat{x}k_x + \hat{y}k_y) \\
d_{A_{2u}}(\mathbf{k}) &= \psi_0(\mathbf{k})(\hat{x}k_y - \hat{y}k_x) \\
d_{B_{1u}}(\mathbf{k}) &= \psi_0(\mathbf{k})(\hat{x}k_x - \hat{y}k_y) \\
d_{B_{2u}}(\mathbf{k}) &= \psi_0(\mathbf{k})(\hat{x}k_y + \hat{y}k_x) \\
d_{E_u}(\mathbf{k}) &= \psi_0(\mathbf{k})\{\hat{z}k_x, \hat{z}k_y\}.
\end{aligned} \tag{M13}$$

here listed in the convenient \mathbf{d} -vector notation for spin-triplet pairing states (see [68]). It is important to note that all composite phases from combination of two pairing states of one-dimensional representation are c -axis equal spin state and would be in agreement with present time NMR Knight data [24, 25] and had been proposed as possible states in Refs. 69, 70. These states are also called helical state in literature, as they are topologically non-trivial with helical surface states. The Knight shift experiments disagree with expectations of the state in representation E_u which yields the chiral p -wave state.

Again we have to make composite states of the one-dimensional representation to obtain TRSB phases. Analogous to the even-parity case we do not find any composite state which satisfies both selection rules, in contrast to the chiral p -wave state which behaves the same way as the chiral d -wave state in this respect.

DATA AVAILABILITY

The data represented in Figs. 2 – 4 are available as Source Data. All other data that support the plots within this paper and other findings of this study are available from the corresponding author upon reasonable request.

ACKNOWLEDGMENTS

The work was performed at the Swiss Muon Source ($S\mu S$), Paul Scherrer Institute (PSI, Switzerland). We acknowledge fruitful discussions with Zurab Guguchia, Carsten Timm, and Jing Xia. Matthias Elender is acknowledged for technical support. The work of R.G. is supported by the Swiss National Science Foundation (SNF Grant No. 200021-175935). The work of M.S and B.Z was financially supported by the Swiss National Science Foundation (SNSF) through Division II (Grant No. 184739). The work of V. G. was supported by DFG GR 4667/1. N.K. acknowledges the support from JSPS KAKENHI (No. JP18K04715) in Japan. Y.M. acknowledges funding by JSPS-CNR-SPIN Core-to-core program

on oxide superspin project, and by JSPS KAKENHI Nos. JP15H05852, JP15K21717, and JP17H06136. The work of H.-H.K was supported by DFG SFB 1143 and GRK 1621.

AUTHOR INFORMATION

Author contributions

R.K, V.G, and M.S conceived the project. Data were taken by R.K, V.G. D.D, and R.G. R.K and V.G performed data analysis and interpreted the results together with M.S.. B.Z. and M.S. provided the theoretical analysis. N.K. provided and characterized samples. R.K., V.G., M.S., and C.W.H. wrote the manuscript with inputs from all authors.

Corresponding Authors

Correspondence to Vadim Grinenko or Manfred Sigrüst or Rustem Khasanov.

ETHICS DECLARATIONS

Competing interests

The authors declare no competing interests.

* Electronic address: v.grinenko@ifw-dresden.de

† Electronic address: mansigri@ethz.ch

‡ Electronic address: rustem.khasanov@psi.ch

- [1] Heffner, R. H., Willis, J. O., Smith, J. L., Birrer, P., Baines, C., Gygax, F. N., Hitti, B., Lippelt, E., Ott, H. R., Schenck, A. & MacLaughlin D. E. Muon-spin relaxation studies of weak magnetic correlations in $U_{1-x}Th_xBe_{13}$. *Phys. Rev. B* **40**, 806(R) (1989).
- [2] Jin, D. S., Carter, S. A., Ellman, B., Rosenbaum, T. F. & Hinks, D. G. Uniaxial-stress anisotropy of the double superconducting transition in UPT_3 . *Phys. Rev. Lett.* **68**, 1597 (1992).
- [3] Luke, G. M., Keren, A., Le, L. P., Wu, W. D., Uemura, Y. J., Bonn, D. A., Taillefer, L. & Garrett, J. D. Muon spin relaxation in UPT_3 . *Phys. Rev. Lett.* **71**, 1466 (1993).
- [4] Riseborough, P. & Smith, J.L. Heavy-Fermion Superconductivity. *The Physics of Superconductors Vol II*, eds. K.H. Bennemann & J.B. Ketterson (2002).
- [5] Maisuradze, A., Schnelle, W., Khasanov, R., Gumeniuk, R., Nicklas, M., Rosner, H., Leithe-Jasper, A., Grin, Yu., Amato, A. & Thalmeier, P. Evidence for time-reversal symmetry breaking in superconducting $PrPt_4Ge_{12}$. *Phys. Rev. B* **82**, 024524 (2010).
- [6] Hillier, A. D., Quintanilla, J., Mazidian, B., Annett, J. F. & Cywinski, R. Nonunitary Triplet Pairing in the Centrosymmetric Superconductor $LaNiGa_2$. *Phys. Rev. Lett.* **109**, 097001 (2012).
- [7] Biswas, P.K., Luetkens, H., Neupert, T., Stüzer, T., Baines, C., Pascua, G., Schnyder, A.P., Fischer, M.H., Goryo, J., Lees, M.R., Maeter, H., Brükner, F., Klauss, H.-H., Nicklas, M., Baker, P.J., Hillier, A.D., Sigrist, M., Amato, A. & Johrendt, D. Evidence for superconductivity with broken time-reversal symmetry in locally noncentrosymmetric $SrPtAs$. *Phys. Rev. B* **87**, 180503 (2013).
- [8] Schemm, E. R., Gannon, W. J., Wishne, C. M., Halperin, W. P. & Kapitulnik, A. Observation of broken time-reversal symmetry in the heavy-fermion superconductor UPt_3 . *Science* **345**, 190 (2014).
- [9] Shang, T., Smidman, M., Ghosh, S. K., Baines, C., Chang, L. J., Gawryluk, D. J., Barker, J. A. T., Singh, R. P., McK. Paul, D., Balakrishnan, G., Pomjakushina, E., Shi, M., Medarde, M., Hillier, A. D., Yuan, H. Q., Quintanilla, J., Mesot, J. & Shiroka, T. Time-Reversal Symmetry Breaking in Re-Based Superconductors, *Phys. Rev. Lett.* **121**, 257002 (2018).
- [10] Ghosh, S.K., Smidman, M., Shang, T., Annett, J.F., Hillier, A.D., Quintanilla, J. & Yuan, H. Recent progress on superconductors with time-reversal symmetry breaking. *J. Phys.: Condens. Matter* **33**, 033001 (2021).
- [11] Grinenko, V., Sarkar, R., Kihou, K., Lee, C. H., Morozov, I., Aswartham, S., Büchner, B., Chekhonin, P., Skrotzki, W., Nenkov, K., Hühne, R., Nielsch, K., Drechsler, S. L., Vadimov, V. L., Silaev, M. A., Volkov, P. A., Eremin, I., Luetkens, H. & Klauss, H.-H. Superconductivity with broken time-reversal symmetry inside a superconducting s -wave state. *Nat. Phys.* **16**, 789-794 (2020).
- [12] Boehm, T., Kemper, A. F., Moritz, B., Kretzschmar, F., Muschler, B., Eiter, H. M., Hackl, R., Devereaux, T. P., Scalapino, D. J. & Wen, H.-H. Balancing Act: Evidence for a Strong Subdominant d-Wave Pairing Channel in $Ba_{0.6}K_{0.4}Fe_2As_2$. *Phys. Rev. X* **4**, 041046 (2014).
- [13] Maeno, Y., Hashimoto, H., Yoshida, K., Nishizaki, S., Fujita, T., Bednorz, J., & Lichtenberg, F. Superconductivity in a layered perovskite without copper. *Nature* **372**, 532-534 (1994).
- [14] Mackenzie, A. P. & Maeno, Y. The superconductivity of Sr_2RuO_4 and the physics of spin-triplet pairing. *Reviews of Modern Physics* **75**, 657 (2003).
- [15] Luke, G. M., Fudamoto, Y., Kojima, K. M., Larkin, M. I., Merrin, J., Nachumi, B., Uemura, Y. J., Maeno, Y., Mao, Z. Q., Mori, Y., Nakamura, H. & Sigrist, M. Time-reversal symmetry-breaking superconductivity in Sr_2RuO_4 . *Nature* **394**, 558-561 (1998).
- [16] Xia, J., Maeno, Y., Beyersdorf, P. T., Fejer, M. M. & Kapitulnik, A. High Resolution Polar Kerr Effect Measurements of Sr_2RuO_4 : Evidence for Broken Time-Reversal Symmetry in the Superconducting State. *Phys. Rev. Lett.* **97**, 167002 (2006).
- [17] Nelson, K.D., Mao, Z.Q., Maeno, Y. & Liu, Y. Odd-parity superconductivity in Sr_2RuO_4 . *Science* **306**, 1151 (2004).
- [18] Kidwingira, F., Strand, J.D., Van Harlingen, D.J. & Maeno, Y. Dynamical Superconducting Order Parameter Domains in Sr_2RuO_4 . *Science* **314**, 1267 (2006).
- [19] Nakamura, T., Sumi, T., Yonezawa, S., Terashima, T., Sigrist, M., Kaneyasu, H. & Maeno, Y. Essential Configuration of Pb/Ru/ Sr_2RuO_4 Junctions Exhibiting Anomalous Superconducting Interference. *J. Phys. Soc. Jpn.* **81**, 064708 (2012).
- [20] Anwar, M. A., Nakamura, T., Yonezawa, S., Yakabe, M., Ishiguro, R., Takayanagi, H. & Maeno, Y. Anomalous switching in Nb/Ru/ Sr_2RuO_4 topological junctions

- by chiral domain wall motion. *Scientific Reports* **3**, 2480 (2013).
- [21] Maeno, Y., Kittaka, S., Nomura, T., Yonezawa, S. & Ishida, K. Evaluation of Spin-Triplet Superconductivity in Sr_2RuO_4 . *J. Phys. Soc. Jpn.* **81**, 011009 (2012).
- [22] Yonezawa, S. and Kajikawa, T. & Maeno, Y. First-Order Superconducting Transition of Sr_2RuO_4 . *Phys. Rev. Lett.* **110**, 077003 (2013).
- [23] Kittaka, S., Kasahara, A., Sakakibara, T., Shibata, D., Yonezawa, S., Maeno, Y., Tenya, K. & Machida, K. Sharp magnetization jump at the first-order superconducting transition in Sr_2RuO_4 . *Phys. Rev. B* **90**, 220502 (2014).
- [24] Pustogow, A., Luo, Y., Chronister, A., Su, Y.-S., Sokolov, D. A., Jerzembeck, F., Mackenzie, A. P., Hicks, C. W., Kikugawa, N., Raghu, S., Bauer, E. D. & Brown, S. E. Constraints on the superconducting order parameter in Sr_2RuO_4 from oxygen-17 nuclear magnetic resonance. *Nature* **574**, 72-75 (2019).
- [25] Ishida, K., Manago, M. & Maeno, Y. Reduction of the ^{17}O Knight Shift in the Superconducting State and the Heat-up Effect by NMR Pulses on Sr_2RuO_4 . *J. Phys. Soc. Jpn.* **89**, 034712 (2020).
- [26] Suh, H. G., Menke, H., Brydon, P. M. R., Timm, C., Ramires, A. & Agterberg, D. F. Stabilizing even-parity chiral superconductivity in Sr_2RuO_4 . *Phys. Rev. Research* **2**, 032023(R) (2020).
- [27] Kasahara, Y., Iwasawa, T., Shishido, H., Shibauchi, T., Behnia, K., Haga, Y., Matsuda, T. D., Onuki, Y., Sigrist, M. & Matsuda Y. Exotic Superconducting Properties in the Electron-Hole-Compensated Heavy-Fermion 'Semimetal' URu_2Si_2 . *Phys. Rev. Lett.* **99**, 116402 (2007).
- [28] Schemm, E. R., Baumbach, R. E., Tobash, P. H., Ronning, F., Bauer, E. D. & Kapitulnik, A. Evidence for broken time-reversal symmetry in the superconducting phase of URu_2Si_2 . *Phys. Rev. B* **91**, 140506(R) (2015).
- [29] Rømer, A. T., Scherer, D. D., Eremin, I. M., Hirschfeld, P. J. & Andersen, B. M. Knight Shift and Leading Superconducting Instability from Spin Fluctuations in Sr_2RuO_4 . *Phys. Rev. Lett.* **123**, 247001 (2019).
- [30] Rømer, A. T., Kreisel, A., Müller, M. A., Hirschfeld, P. J., Eremin, I. M. & Andersen, B. M. Theory of strain-induced magnetic order and splitting of T_c and T_{TRSB} in Sr_2RuO_4 . *Phys. Rev. B* **102**, 054506 (2020).
- [31] Kivelson, S. A., Yuan, A. C., Ramshaw, B. & Thomale, R. A proposal for reconciling diverse experiments on the superconducting state in Sr_2RuO_4 . *npj Quantum Mat.* **5**, 43 (2020).
- [32] Willa, R. Symmetry-mixed bound-state order. *Phys. Rev. B* **102**, 180503(R) (2020).
- [33] Zinkl, B. & Sigrist, M. Impurity induced double transitions for accidentally degenerate unconventional pairing states. *Phys. Rev. Research* **3**, L012004 (2021).
- [34] Andreica, D. Magnetic phase diagram in some Kondo-lattice compounds. PhD thesis, ETH Zürich, 2001.
- [35] Khasanov, R., Guguchia, Z., Maisuradze, A., Andreica, D., Elender, M., Raselli, A., Shermadini, Z., Goko, T., Morenzoni, E. & Amato, A. High pressure research using muons at the Paul Scherrer Institute. *High Pressure Res.* **36**, 140-166 (2016).
- [36] Shermadini, Z., Khasanov, R., Elender, M., Simutis, G., Guguchia, Z., Kamenev, K. V. & Amato, A. A low-background piston cylinder-type hybrid high pressure cell for muon-spin rotation/relaxation experiments. *High Pressure Res.* **37**, 449 (2017).
- [37] Murata, K., Yoshino, H., Yadav, H. O., Honda Y. & Shirakawa, N. Pt resistor thermometry and pressure calibration in a clamped pressure cell with the medium, Daphne 7373. *Rev. Sci. Instrum.* **68**, 2490-2493 (1997).
- [38] Steppke, A., Zhao, L., Barber, M. E., Scaffidi, T., Jerzembeck, F., Rosner, H., Gibbs, A. S., Maeno, Y., Simon, S. H., Mackenzie, A. P. & Hicks, C. W. Strong peak in T_c of Sr_2RuO_4 under uniaxial pressure. *Science* **355**, eaaf9398 (2017).
- [39] Hatlo, M. et al. Developments of mathematical software libraries for the LHC experiments. *IEEE Trans. Nucl. Sci.* **52**, 2818-2822 (2005).
- [40] Bobowski, J. S., Kikugawa, N., Miyoshi, T., Suwa, H., Xu, H.-S., Yonezawa, S., Sokolov, D. A., Mackenzie, A. P. & Maeno, Y. Improved Single-Crystal Growth of Sr_2RuO_4 . *Condensed Matter* **4**, 6 (2019).
- [41] Yaouanc, A. & Dalmas de Réotier, P. Muon Spin Rotation, Relaxation and Resonance: Applications to Condensed Matter. Oxford University Press, Oxford, 2011.
- [42] Weber, M., Amato, A., Gygax, F. N., Schenck, A., Maletta, H., Duginov, V. N., Grebinnik, V. G., Lazarev, A. B., Olshevsky, V. G., Pomjakushin, V. Yu., Shilov, S. N., Zhukov, V. A., Kirillov, B. F., Pirogov, A. V., Ponomarev, A. N., Storchak, V. G., Kapusta, S. & Bock, J. Magnetic-flux distribution and the magnetic penetration depth in superconducting polycrystalline $\text{Bi}_2\text{Sr}_2\text{Ca}_{1-x}\text{Y}_x\text{Cu}_2\text{O}_{8+\delta}$ and $\text{Bi}_{2-x}\text{Pb}_x\text{Sr}_2\text{CaCu}_2\text{O}_{8+\delta}$. *Phys. Rev. B* **48**, 13022 (1993).
- [43] Khasanov, R., Zhou, H., Amato, A., Guguchia, Z., Morenzoni, E., Dong, X., Zhang, G. & Zhao, Z. Proximity-induced superconductivity within the insulating $(\text{Li}_{0.84}\text{Fe}_{0.16})\text{OH}$ layers in $(\text{Li}_{0.84}\text{Fe}_{0.16})\text{OHFe}_{0.98}\text{Se}$. *Phys. Rev. B* **93**, 224512 (2016).
- [44] Shirakawa, N., Murata, K., Nishizaki, S., Maeno, Y. & Fujita, T. Pressure dependence of superconducting critical temperature of Sr_2RuO_4 . *Phys. Rev. B* **56**, 7890 (1997).
- [45] Forsythe, D., Julian, S. R., Bergemann, C., Pugh, E., Steiner, M. J., Alireza, P. L., McMullan, G. J., Nakamura, F., Haselwimmer, R. K. W., Walker, I. R., Saxena, S. S., Lonzarich, G. G., Mackenzie, A. P., Mao, Z. Q. & Maeno, Y. Evolution of Fermi-Liquid Interactions in Sr_2RuO_4 under Pressure. *Phys. Rev. Lett.* **89**, 166402 (2002).
- [46] Svitelskiy, O., Headley, S., Tozer, S. W., Palm, E. C., Murphy, T. P., Shulyatev, D. & Suslov, A. V. Influence of hydrostatic pressure on the magnetic phase diagram of superconducting Sr_2RuO_4 by ultrasonic attenuation. *Phys. Rev. B* **77**, 052502 (2008).
- [47] Luke, G. M., Fudamoto, Y., Kojima, K. M., Larkin, M. I., Nachumi, B., Uemura, Y. J., Sonier, J. E., Maeno, Y., Mao, Z. Q., Mori, Y. & Agterberg, D. F. Unconventional superconductivity in Sr_2RuO_4 . *Physica B* **289-290**, 373-376 (2000).
- [48] Grinenko, V., Ghosh, S., Sarkar, R., Orain, J.-C., Nikitin, A., Elender, M., Das, D., Guguchia, Z., Brückner, F., Barber, M. E., Park, J., Kikugawa, N., Sokolov, D. A., Bobowski, J. S., Miyoshi, T., Maeno, Y., Mackenzie, A. P., Luetkens, H., Hicks, C. W. & Klauss, H.-H. Split superconducting and time-reversal symmetry-breaking transitions, and magnetic order in Sr_2RuO_4 under stress. To appear in *Nature Phys.* <https://doi.org/10.1038/s41567-021-01182-7>
- [49] Shiroka, T., Fittipaldi, R., Cuocco, M., De Renzi, R., Maeno, Y., Lycett, R. J., Ramos, S., Forgan, E. M., Baines, C., Rost, A., Granata, V. & Vecchione, A. μSR studies of superconductivity in eutectically grown mixed

- ruthenates. *Phys. Rev. B* **85**, 134527 (2012).
- [50] Higemoto, W., Koda, A., Kadono, R., Yoshida, Y. & Onuki, Y. Investigation of Spontaneous Magnetic Field in Spin-Triplet Superconductor Sr_2RuO_4 . *JPS Conference Proceedings* **2**, 010202 (2014).
- [51] Li, Y.-S., Kikugawa, N., Sokolov, D. A., Jerzembeck, F., Gibbs, A. S., Maeno, Y., Hicks, C. W., Nicklas, M. & Mackenzie, A. P. High sensitivity heat capacity measurements on Sr_2RuO_4 under uniaxial pressure. *PNAS* **118** e2020492118; <https://doi.org/10.1073/pnas.2020492118>
- [52] Kikugawa, N., Mackenzie, A. P., Bergemann, C., Borzi, R. A., Grigera, S. A. & Maeno, Y. Rigid-band shift of the Fermi level in the strongly correlated metal: $\text{Sr}_{2-y}\text{La}_y\text{RuO}_4$. *Phys. Rev. B* **70**, 060508(R) (2004).
- [53] Shen, K. M., Kikugawa, N., Bergemann, C., Balicas, L., Baumberger, F., Meevasana, W., Ingle, N. J. C., Maeno, Y., Shen, Z.-X. & Mackenzie, A. P. Evolution of the Fermi Surface and Quasiparticle Renormalization through a van Hove Singularity in $\text{Sr}_{2-y}\text{La}_y\text{RuO}_4$. *Phys. Rev. Lett.* **99**, 187001 (2007).
- [54] Bud'ko, S. L., Ni, Ni & Canfield, P. C. Jump in specific heat at the superconducting transition temperature in $\text{Ba}(\text{Fe}_{1-x}\text{Co}_x)_2\text{As}_2$ and $\text{Ba}(\text{Fe}_{1-x}\text{Ni}_x)_2\text{As}_2$ single crystals. *Phys. Rev. B* **79**, 220516(R) (2009).
- [55] Kirtley, J. R., Kallin, C., Hicks, C. W., Kim, E.-A., Liu, Y., Moler, K. A., Maeno, Y. & Nelson, K. D. Upper limit on spontaneous supercurrents in Sr_2RuO_4 . *Phys. Rev. B* **76**, 014526 (2007).
- [56] Curran, P. J., Bending, S. J., Desoky, W. M., Gibbs, A. S., Lee, S. L. & Mackenzie, A. P. Search for spontaneous edge currents and vortex imaging in Sr_2RuO_4 mesostructures. *Phys. Rev. B* **89**, 144504 (2014).
- [57] Ghosh, S., Shekhter, A., Jerzembeck, F., Kikugawa, N., Sokolov, D. A., Mackenzie, A. P., Hicks, C. W. & Ramshaw, B. J. Thermodynamic evidence for a two-component superconducting order parameter in Sr_2RuO_4 . *Nat. Phys.* **17**, 199–204 (2021); <https://doi.org/10.1038/s41567-020-1032-4>.
- [58] Benhabib, S., Lupien, C., Paul, I., Berges, L., Dion, M., Nardone, M., Zitouni, A., Mao, Z. Q., Maeno, Y., Georges, A., Taillefer, L. & Proust, C. Ultrasound evidence for a two-component superconducting order parameter in Sr_2RuO_4 . *Nat. Phys.* **17**, 194–198 (2021); <https://doi.org/10.1038/s41567-020-1033-3> (2020).
- [59] Walker, M. B. & Contreras, P. Theory of elastic properties of Sr_2RuO_4 at the superconducting transition temperature. *Phys. Rev. B* **66**, 214508 (2002).
- [60] Sigrist, M. Ehrenfest Relations for Ultrasound Absorption in Sr_2RuO_4 . *Progress of Theoretical Physics* **107**, 917 (2002).
- [61] Rømer, A. T., Hirschfeld, P. J. & Andersen, B. M. Superconducting state of Sr_2RuO_4 in the presence of longer-range Coulomb interactions. *arXiv:2101.06972* (2021).
- [62] Zutic, I. & Mazin, I. Phase-Sensitive Tests of the Pairing State Symmetry in Sr_2RuO_4 . *Phys. Rev. Lett.* **95**, 217004 (2005).
- [63] Hassinger, E., Bourgeois-Hope, P., Taniguchi, H., René de Cotret, S., Grissonnanche, G., Anwar, M. S., Maeno, Y., Doiron-Leyraud, N. & Taillefer, L. Vertical Line Nodes in the Superconducting Gap Structure of Sr_2RuO_4 . *Phys. Rev. X* **7**, 011032 (2017).
- [64] Gingras, O., Nourafkan, R., Tremblay, A.-M. S. & Côté, M. Superconducting symmetries of Sr_2RuO_4 from first-principles electronic structure. *Phys. Rev. Lett.* **123**, 217005 (2019).
- [65] Puetter, C. M. & Kee, H.-Y. Identifying spin-triplet pairing in spin-orbit coupled multi-band superconductors. *Europhys. Lett.* **98**, 27010 (2012).
- [66] Khasanov, R., Guguchia, Z., Eremin, I., Luetkens, H., Amato, A., Biswas, P. K., Rüegg, C., Susner, M. A., Sefat, A. S., Zhigadlo, N. D. & Morenzoni, E. Pressure-induced electronic phase separation of magnetism and superconductivity in CrAs . *Scientific Reports* **5**, 13788 (2015).
- [67] Hayano, R. S., Uemura, Y. J., Imazato, J., Nishida, N., Yamazaki, T. & Kubo, R. Zero-and low-field spin relaxation studied by positive muons. *Phys. Rev. B* **20**, 850 (1979).
- [68] Sigrist, M. & Ueda, K. Phenomenological theory of unconventional superconductivity. *Rev. Mod. Phys.* **63**, 239 (1991).
- [69] Kashiwaya, S., Saitoh, K., Kashiwaya, H., Koyanagi, M., Sato, M., Yada, K., Tanaka, Y. & Maeno, Y. Time-reversal invariant superconductivity of Sr_2RuO_4 revealed by Josephson effects. *Phys. Rev. B* **100**, 094530 (2019).
- [70] Ikegaya, S., Yada, K., Tanaka, Y., Kashiwaya, S., Asano, Y. & Manske, D. Identification of spin-triplet superconductivity through a helical-chiral phase transition in Sr_2RuO_4 thin-films. *Phys. Rev. B* **101**, 220501 (2020).